Geophysical Research Letters

RESEARCH LETTER
10.1029/2024GL111159

Tracking Multiyear Sea-Ice Variation in the Arctic Ocean Over Decades With Microseism

Jui-Chun Freya Chen[1], **Sunyoung Park**[1], **and Douglas R. MacAyeal**[1]

[1]Department of the Geophysical Sciences, The University of Chicago, Chicago, IL, USA

Key Points:

- We construct a model of microseism observed in Arctic seismic data that depends on sea-ice concentration and ocean-surface winds
- Sea-ice concentration within 200–300 km of the seismic station, corresponding to the continental slope, affects microseism most strongly
- Microseism power has gradually increased over the last 32 years, reflecting the reduction of Arctic sea ice associated with climate change

Supporting Information:

Supporting Information may be found in the online version of this article.

Correspondence to:

J.-C. F. Chen,
freyachen@uchicago.edu

Citation:

Chen, J.-C. F., Park, S., & MacAyeal, D. R. (2025). Tracking multiyear sea-ice variation in the Arctic ocean over decades with microseism. *Geophysical Research Letters*, *52*, e2024GL111159. https://doi.org/10.1029/2024GL111159

Received 2 JUL 2024
Accepted 19 DEC 2024

Author Contributions:

Conceptualization: Jui-Chun Freya Chen, Sunyoung Park, Douglas R. MacAyeal
Formal analysis: Jui-Chun Freya Chen
Funding acquisition: Sunyoung Park, Douglas R. MacAyeal
Methodology: Jui-Chun Freya Chen, Sunyoung Park, Douglas R. MacAyeal
Supervision: Sunyoung Park, Douglas R. MacAyeal
Validation: Jui-Chun Freya Chen
Visualization: Jui-Chun Freya Chen
Writing – original draft: Jui-Chun Freya Chen
Writing – review & editing: Jui-Chun Freya Chen, Sunyoung Park, Douglas R. MacAyeal

Abstract We construct a linear model of microseism power as a function of sea-ice concentration and ocean-wave activity with a seismic station located on northern Ellesmere Island. The influence of wind-ice-ocean interactions on microseism has been taken into account. We find the increase in microseism power over the last 32 years reflects the long-term loss of sea ice and increasing ocean-wave activity in the Arctic Ocean likely associated with climate change. We further assess model performance to determine a representative region over which sea-ice concentration and ocean-wave activity most directly influence the microseism power. The seismological methods developed here suggest that there is the potential to augment or refine observations of sea-ice conditions obtained from satellites and from *in-situ* observations. Seismological methods may thus help determine properties such as sea-ice thickness, which are less amenable to conventional observations, under a changing climate, particularly in remote areas like the High Arctic.

Plain Language Summary Microseism is a time-continuous signal recorded by seismometers that is related to environmental variables, and originates from ocean-wave activity that excites seismic waves in the seabed. We examine the potential use of microseism to monitor properties of sea ice that may be harder to observe continuously in time with satellites. Here, we develop a simple model that uses the variation of sea-ice concentration and ocean-wave activity to predict microseism energy at a seismic station located in the High Arctic. The success of this model suggests that microseism models can be used as tools to infer sea ice conditions in remote areas even with only one seismic station.

1. Introduction

The reduction of Arctic sea ice is both an important driver and indicator of climate change that is traditionally documented by remote sensing from satellites (e.g., Comiso, 1986; Comiso & Kwok, 1996; Johannessen et al., 1999; Stroeve & Notz, 2018). While this remote-sensing observation has produced compelling evidence of how the Arctic is responding to continued greenhouse gas emissions, there are limitations. For example, estimated sea-ice thickness largely relies on the hydrostatic assumption and estimated snow depth (Ricker et al., 2014; Wadhams et al., 1992). In addition, meltwater ponds on the surface of sea ice can be confused for ice-free ocean areas (Kwok, 2010). Although approaches utilizing coupled ice-ocean models that assimilate observational data have allowed assessment of the Arctic sea-ice extent (Kauker et al., 2009), the results in the summertime are still hard to validate due to lack of summertime observation (Ordoñez et al., 2018). Finally, the temporal resolution of satellite observations is limited (e.g., diurnal to several days), resulting in deficient detection of mesoscale and sub-mesoscale (10 km–10 s of m) dynamics of sea ice which operate on short time scales.

Seismological observation has the potential to mitigate some of the temporal and spatial challenges cited above for satellite observation. Specifically, seismic data provide near-continuous monitoring of ground motions that may be indicative of sea-ice and glaciological processes (e.g., seismic observations have been adapted to high-mountain glacier lake monitoring, Lindner et al., 2020; Maurer et al., 2020). An additional advantage of seismological observation is that seismic instruments are autonomous and do not require constant oversight by human operators as is required, for example, by *in-situ* observation approaches using ground-penetrating radar or drilling. Seismic data, if it can be applied to sea-ice observation, as we shall attempt here, can therefore be a potential complement to conventional observation approaches using satellites and *in-situ* methods.

Here, we investigate the possible applicability of seismological data, specifically microseism, to the observation of sea ice. Microseism is an ever-present, low-amplitude ground vibration generated by ocean wave-derived pressure fluctuations on the seabed between approximately 0.5 and 20 s period (e.g., Hasselmann, 1963; Longuet-Higgins & Jeffreys, 1950; Press & Ewing, 1948). It can be used to address environmental processes (e.g.,

Aster et al., 2023), especially in polar regions where sea ice modifies and attenuates ocean wave propagation through its viscoelastic behavior (Cathles et al., 2009; Stutzmann et al., 2009). In particular, short-period secondary microseism may be the most responsive to sea-ice conditions at the coastal region (Aster et al., 2010; Gimbert & Tsai, 2015). These modulations vary with frequency, and this may provide a means to differentiate those properties of the sea ice that affect generation (e.g., sea-ice concentration) and attenuation (e.g., sea-ice strength) of microseism.

There has been notable success in correlating microseism with sea-ice conditions in the Southern Ocean and the Bering Sea (Anthony et al., 2017; Cannata et al., 2019; Grob et al., 2011a; Tsai & McNamara, 2011); however, efforts to assess this correlation elsewhere in the Arctic Ocean have yet to be tried. The aim of this study is to make this assessment using observed short-period (0.5–2 s) secondary microseism observed by a seismic station on Ellesmere Island (II.ALE (Scripps Institution of Oceanography, 1986) in Figure 1). The use of a single station is notable, as it differs from previous studies that rely on multiple seismic stations (Cannata et al., 2019; Koch et al., 2011; Tsai & McNamara, 2011), particularly given the relatively limited availability of seismic data in the remote High Arctic region. An additional goal of this study is to evaluate the correlation between observed microseism, sea-ice, and ocean conditions in the Arctic Ocean north of the Canadian Archipelago and Greenland where multiyear sea ice is undergoing notable reductions. Our methodology involves a simple linear model that extends the approach of Tsai and McNamara (2011) by including aspects of wind-ice-ocean interactions that may influence microseism power in addition to sea-ice concentration. The sensitivity of the performance of this linear model to sea-ice and ocean conditions within specific distance ranges (e.g., 100–400 km) of the seismic station will also be evaluated.

2. Data and Method

2.1. Study Area

We focus on the part of the Arctic Ocean north of Ellesmere Island because this location is the "Last Ice Area" to where multiyear sea ice has been retreating from its previous broad coverage of the Arctic Ocean. In other words, our study area is the refugium to which multiyear sea ice is retreating (Meier et al., 2014). Located on Ellesmere Island, at Alert, Nunavut, Canada, is a permanent seismic station (II.ALE) of the Global Seismographic Network (GSN) that has operated since 1991 (Ringler et al., 2022) (Figures 1c–1f, red triangle). The seismic station is located in the near-shore area, which reduces attenuation through the land and provides reliable observation of microseism (Bromirski & Duennebier, 2002; Cessaro, 1994). The sea ice and ocean data around the station as described in the following sections are then used to compare with the seismic data (Figure 2).

2.2. Sea-Ice Concentration

We use daily data from the passive microwave satellite records (Nimbus-7 SMMR and DMSP SSM/I-SSMIS, Version 2) with 25 × 25 km spatial resolution made available by the US National Snow and Ice Data Center (NSIDC) (DiGirolamo et al., 2022). Figures 1d and 1f highlight the contrast of sea-ice concentration between a winter day that had nearly 100% of sea-ice cover and a summer day with less sea ice. Assuming sea-ice concentration within a certain distance range D from the seismic station influences microseism power (Tsai & McNamara, 2011), we use the average sea-ice concentration within the distance D from ALE. The value of D is varied as part of optimizing the model we develop here (see Section 3.1) to assess the spatial domain over which a single seismic station is sensitive to sea-ice conditions. As the sea-ice concentration data is unavailable around the North Pole (e.g., 87.2 − 90° N) due to the orbit inclination of the satellites, we explore the distance D up to 400 km. Once the spatially averaged sea-ice concentration is evaluated from the NSIDC data on a day-by-day basis, it is then time filtered using a 7-day moving average to eliminate day-to-day variations. This spatially averaged, time-filtered sea ice data is denoted by the variable $S(t)$, where t is time (Figure 2c).

2.3. Microseism

We compile a 20-year record of short-period (0.1–10 s) microseism observed at II. ALE from data retrieved from the US Data Management Center (DMC) of the seismological consortium EarthScope. This data is then compared with $S(t)$ in order to determine the frequency band where the variation in microseism power is most correlated with the variation of sea ice.

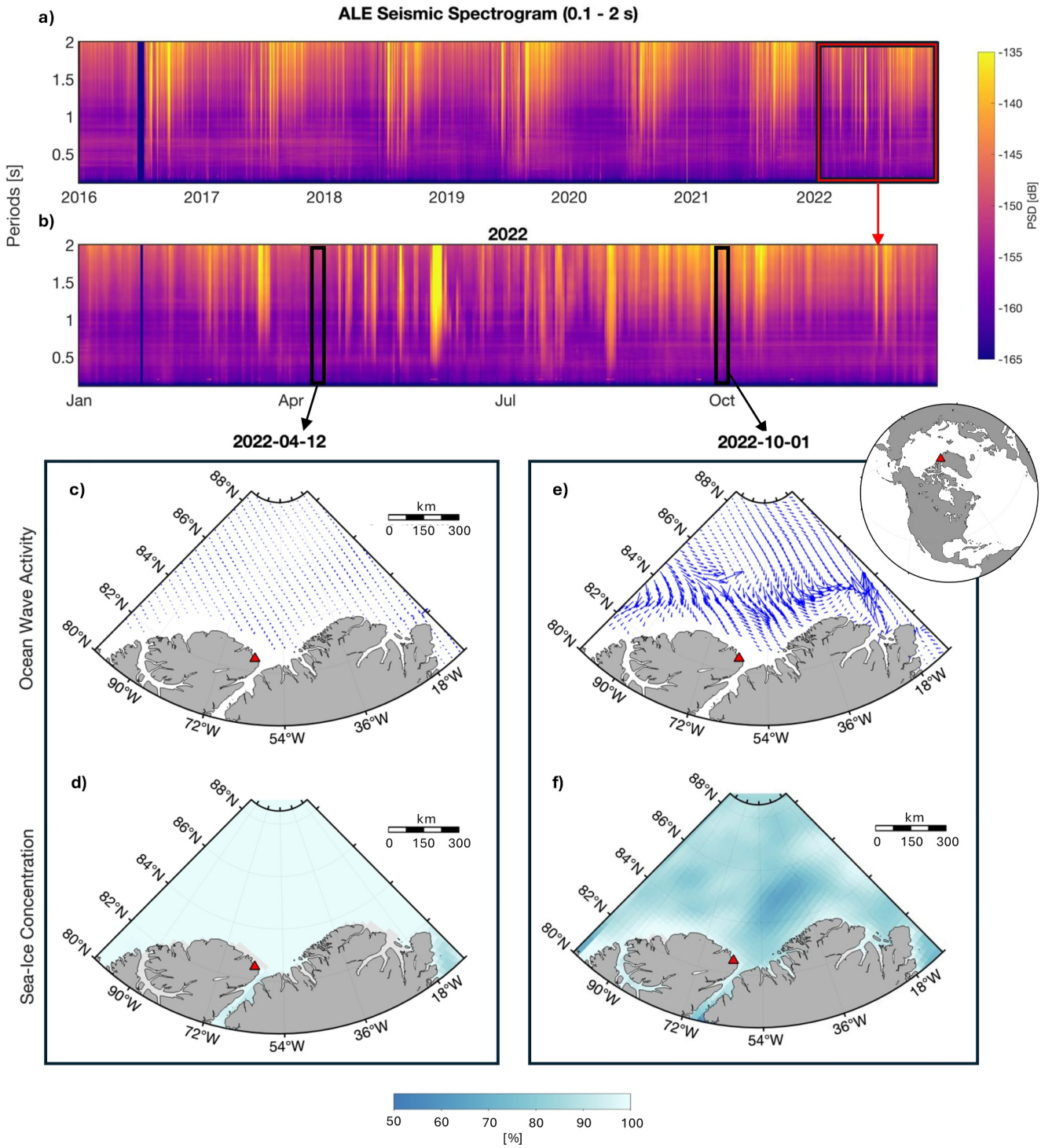

Figure 1. Spectrogram of microseism in the 0.1 − 2 s period range at station ALE over (a) 2016–2022 and (b) 2022. Derived ocean-wave activity used to generate $\vec{U}_o$ and sea-ice concentration used to generate $\vec{S}$ around station ALE (red triangles) for 2022-04-12 and 2022-10-01 (c)–(f).

The seismic data have a 20 Hz sampling rate and are recorded by Streckeisen STS-1 seismic sensors with a flat response within 0.1 − 100 s period range (Scripps Institution of Oceanography, 1986). As Rayleigh waves account for most microseism and dominate the vertical component of ground motion, we focus on the vertical component of the seismic records (Gualtieri et al., 2020; Haubrich & McCamy, 1969). The instrumental response

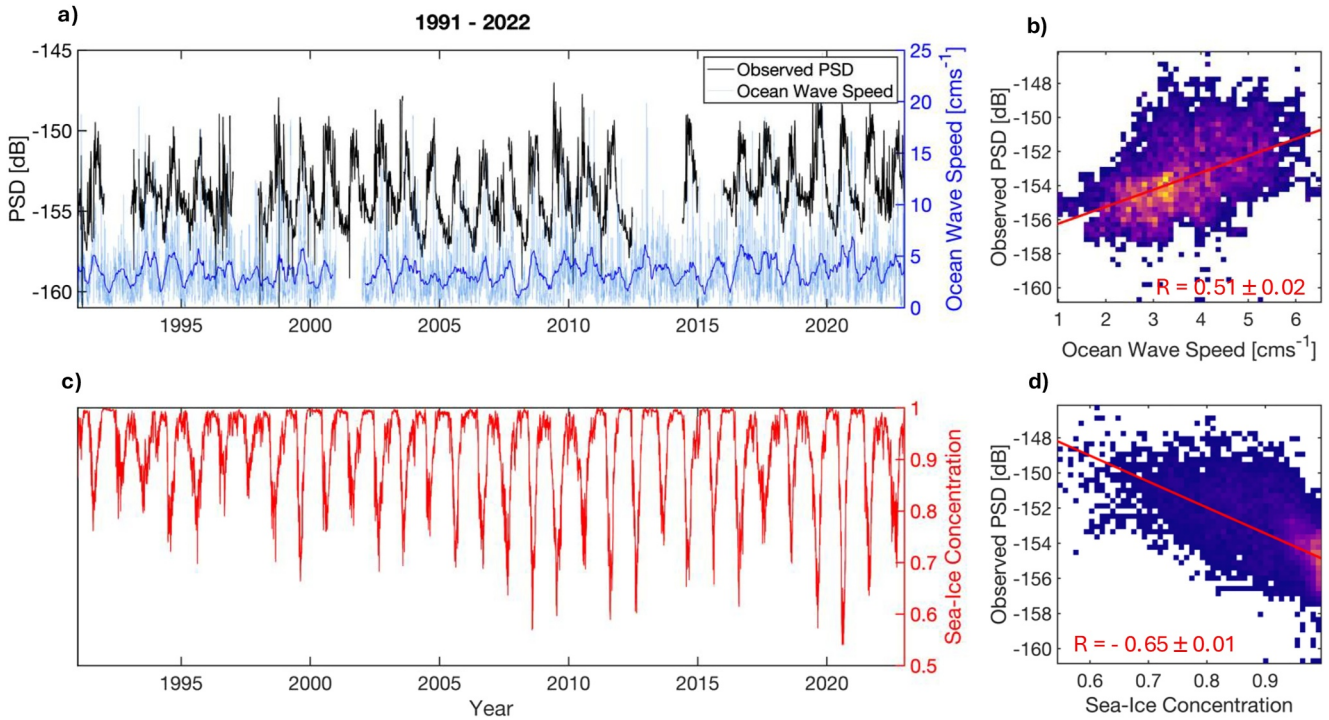

Figure 2. Comparison of observed microseism power (in dB) in the 0.1 − 2 s period band (black line in a) with (a) ocean (light blue line for 7-day moving averaged and dark blue line for 90-day moving averaged) and (c) sea-ice data at $D = 400$ km. Correlation between observed microseism power and $U_o(t)$ and $S(t)$ (b and d, respectively). Red lines show the linear regressions and their corresponding correlation coefficients.

is removed from the data after being demeaned and detrended using ObsPy software. We process in total 32 years (1991 − 2022) of seismic data to track the long-term variation of microseism and its relationship with sea ice.

To explore the time-frequency characteristics of seismic records at ALE, we examine the daily averaged spectrogram of seismic data created using a Short-Time Fourier Transform (STFT) every 50 s with 70% overlapping data segments. In Figure S2a in Supporting Information S1, seismic Power Spectral Density (PSD) in the long-period range (with period >2 s) shows seasonal changes where the highest and lowest PSD occurs in the wintertime and summertime, respectively. This can be caused by the overall stormier weather conditions in the winter of the Arctic region and its surrounding oceans (Grob et al., 2011b) and the long-distance propagation of longer-period Rayleigh waves. Short-period PSD (with a period below about 2 s)—corresponding to the secondary microseism excited by the ocean-wave interference (Ardhuin et al., 2011)—shows the opposite seasonal pattern from the long-period PSD, high in summer and low in winter with an abrupt increase in early summer (Figure 1a and Figure S2b in Supporting Information S1). This can be due to the attenuating effects of sea ice on short-period, short-wavelength ocean waves (Sergeant et al., 2013).

During the period from November to mid-June, the sea-ice concentration mostly varies within 1.0 − 0.95 (e.g., Figure 1d). An abrupt decrease of sea-ice concentration begins in early July, which matches the sudden increase of seismic power within the approximate 0.1 − 2.0 s period range (Figures 1a and 1b). Based on this seasonal characteristic and the high correlation with sea-ice concentration (−0.65 in Figure 2d), we hypothesize that microseism recorded at ALE within this period range is highly sensitive to the variation of sea ice around the station, consistent with the similar period range found by Tsai and McNamara (2011) in the Bering Sea region. We utilize averaged PSD within this period range for our following analyses and discussion, and denote it as $P(t)$. As with the sea-ice concentration data $S(t)$, a 7-day moving average is applied to the PSD to obtain $P(t)$ over 32 years (Figure 2a black line).

2.4. Ocean-Wave Activity in Ice-Covered Ocean

Ocean-wave activity is the primary generator of microseism, but ocean waves are difficult to directly observe in the Arctic Ocean. To represent the microseism source term in the model, an empirically determined proxy variable taking into account the momentum transfer between surface wind and sea-ice motion is used. This approach has been suggested by several observational studies that are based on comparisons between remotely sensed wind and sea-ice drift (Heorton et al., 2019; Kimura, 2004; Kimura & Wakatsuchi, 2000). We use the geostrophic surface-wind vector $\vec{U}_g$ and the observed sea-ice motion vector $\vec{U}_i$ to evaluate an empirical surface-ocean vector field, $\vec{U}_o$, the magnitude of which, $|\vec{U}_o|$, will be used as the proxy variable for ocean-wave activity (microseism-generation term). This vector field is related to $\vec{U}_g$ and $\vec{U}_i$ by,

$$\vec{U}_o = \vec{U}_i - \mathbf{F} \cdot \vec{U}_g \tag{1}$$

where $\mathbf{F}$ is a linear transformation that both rotates and attenuates the geostrophic wind $\vec{U}_g$. Following Kimura and Wakatsuchi (2000), we assume $\mathbf{F}$ is a complex coefficient involving an ice speed reduction factor $|F|$ and turning angle θ:

$$\mathbf{F} = |F| e^{-i\theta}. \tag{2}$$

We use ERA5-reanalysis 1,000 hPa 10 km hourly wind data for $\vec{U}_g$ (Hersbach et al., 2023), and daily sea-ice motion data (Polar Pathfinder Daily 25 km EASE-Grid Sea Ice Motion Vectors, Version 4) from NSIDC for $\vec{U}_i$ (Tschudi et al., 2019) and apply a 7-day moving average to both, consistent with the smoothing performed for seismic and sea-ice concentration data.

We can see from Figures 1c and 1e, that $\vec{U}_o$ has low magnitude when the ocean is covered by sea ice, and becomes large when there is more open water exposed to the surface winds. The derived $|\vec{U}_o|$ (light blue line in Figure 2a) is then averaged over the distance D from the seismic station and time-filtered with a 90-day moving average to reduce stochastic day-to-day noise. The result of this averaging is denoted by the variable U_o. By doing so, the noise level becomes comparable between $U_o(t)$ and $P(t)$ and appears to have similar seasonal variations (dark blue and black lines in Figure 2a). The spatially averaged, time-filtered $U_o(t)$ is then used in the model derived below.

2.5. Linear Parameterized Model of Microseism Power

We construct a simple linear model that relates $P(t)$ to $S(t)$ and $U_o(t)$ to determine how microseism power variation at ALE is influenced by sea-ice and ocean conditions. To do so, we assess the correlations between these parameters. The seasonality of $U_o(t)$ matches well with that of microseism power $P(t)$ with a correlation coefficient of 0.51 (Figure 2b). The sea-ice concentration $S(t)$ is negatively correlated to $P(t)$ with a correlation coefficient of -0.65 (Figure 2d). The negative correlation coefficient indicates an inverse relationship between $S(t)$ and $P(t)$, that is, the more sea-ice concentration the less microseism power.

With the results of the above statistical analysis, we establish a linear model of microseism power at ALE:

$$P(t) = \beta_0 + \beta_1 \cdot U_o(t) + \beta_2 \cdot S(t) + \epsilon(t) \tag{3}$$

where the coefficients β_0, β_1 and β_2 are determined from linear least-squares regression, and $\epsilon(t)$ is the residual error. The performance of the model is then assessed by comparing the observed microseism power (P) against the modeled microseism power $\left(\hat{P}\right)$. The correlation coefficient (CC), the root-mean-square error (RMSE) and the R^2 are explored to quantify the comparison:

$$CC = \frac{\langle \hat{P}, P \rangle}{\sigma(\hat{P})\sigma(P)} \tag{4}$$

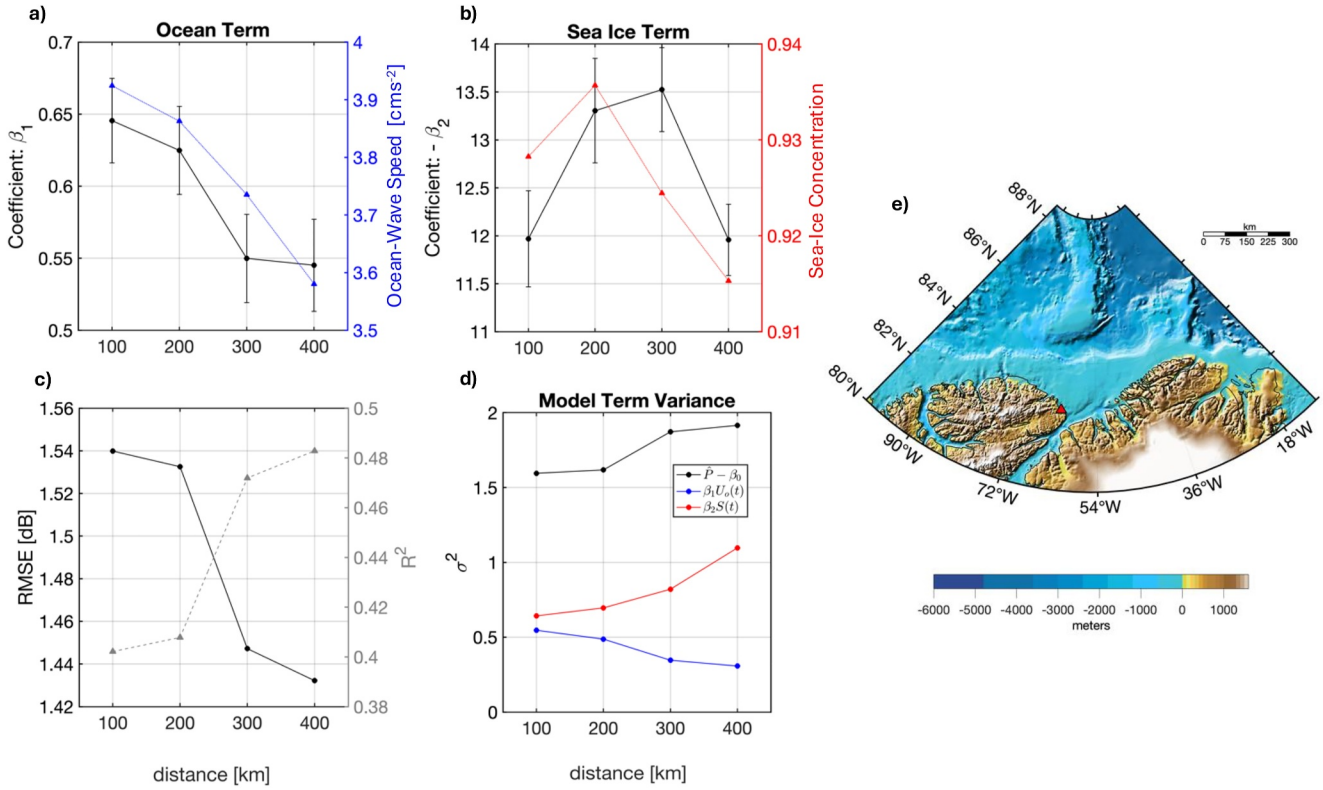

Figure 3. Model performance as a function of data-input domain radius D (horizontal axes, km). (a) Ocean-term coefficients β_1 (black line) with error bars of 95% confident interval and total U_o (blue line) as functions of D. (b) Sea-ice-term coefficients β_2 (black line) with error bars same as in (a) and total S (red line) as functions of D. (c) Root-mean squared (RMSE) difference between the model and observed microseism amplitude (black line) and the R^2 (gray dashed line) of each model as functions of D. (d) The variance of terms in Equation 3 as functions of D. (e) Bathymetry map near ALE (red triangle).

$$RMSE = \sqrt{\frac{(\hat{P} - P)^2}{N}} \tag{5}$$

$$R^2 = 1 - \frac{\sum^N (P - \hat{P})^2}{\sum^N (P - \overline{P})^2} \tag{6}$$

where $\bar{P}$ is the averaged P over time, $\langle\ ,\ \rangle$ refers to the covariance operator, σ is the standard deviation operator and the number of time steps predicted by the model is indicated by N.

3. Results

3.1. Model Performance as a Function of Domain Size

To explore the distance D within which sea-ice concentration and ocean-momentum transfer explain the microseism power at ALE most accurately, we compare modeling results for different distance ranges from the seismic station. The statistical analysis of each model result is shown in Figure 3. Coefficients β_1 and β_2 and their uncertainties determined by least squares optimization are shown in black lines and error bars, respectively, in Figures 3a and 3b (See Text S1 in Supporting Information S1 and Figure S1 in Supporting Information S1 for the covariance discussions). β_1 and β_2 are larger when D is within 100 − 200 km and 200 − 300 km, respectively. Additionally, the ocean-wave activity (blue line in Figure 3a) and sea-ice concentration (red line in Figure 3b) are both highest for D = 100 or 200 km. These suggest that the microseism power at ALE is largely controlled by regional conditions in ocean wave power and sea ice.

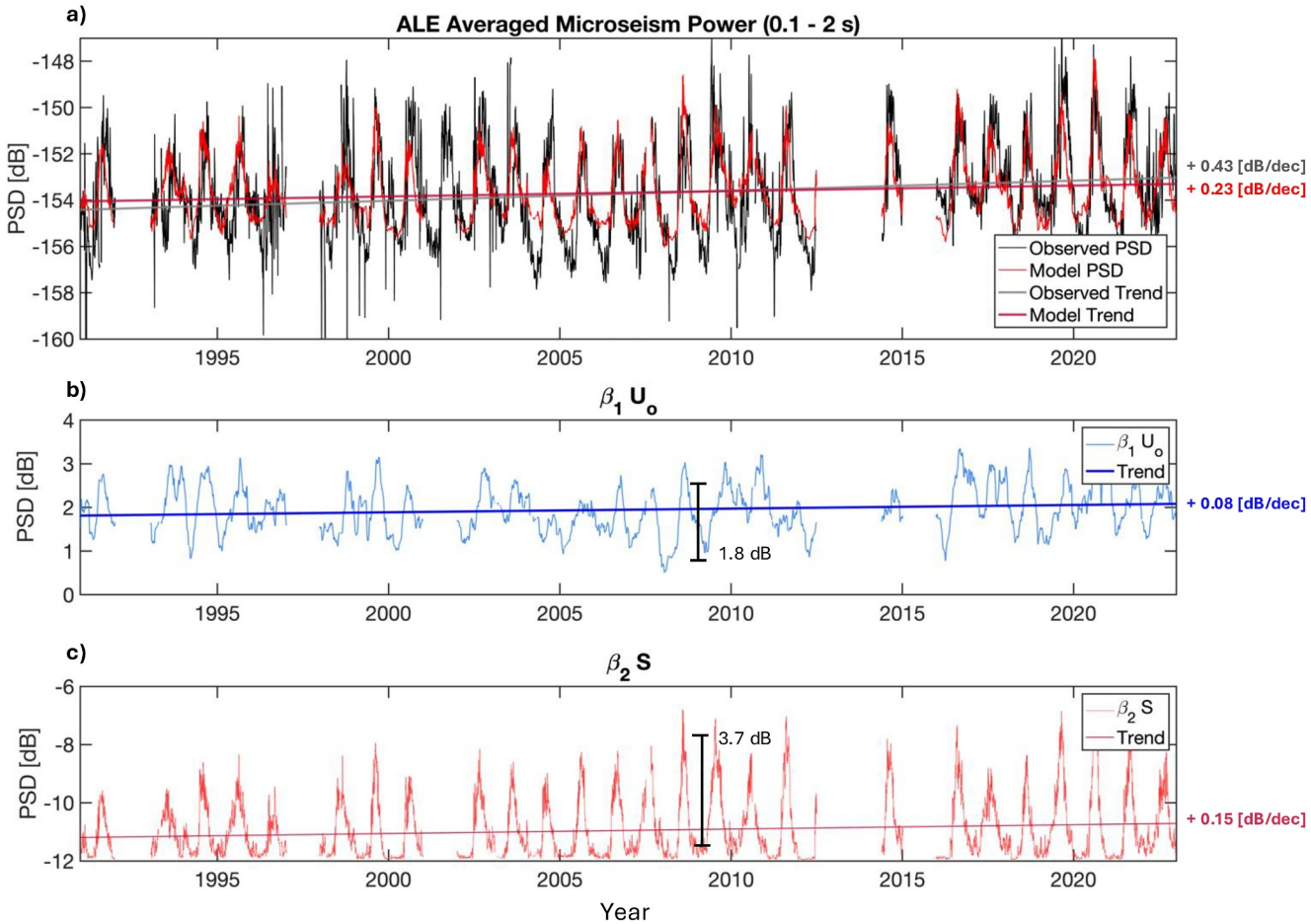

Figure 4. Model performance as a function of time over the period 1991–2022 with linear trends indicated. (a) Observed (black line) and modeled (red line) microseism power (in dB) at ALE in the period range of 0.1–2 s for $D = 400$ km. (b) Ocean contribution to microseism $(\beta_1 U_o(t))$. (c) Sea-ice contribution to microseism $(\beta_2 S(t))$. Trends of the variables are indicated (associated by color) on the right-hand side of each panel and by thick straight lines.

Even though the nearest conditions are affecting the microseism the most, we find that the relatively farther-away conditions of ocean and sea ice are still important for explaining the microseism power. The RMSE (Figure 3c, black line) is about 1.54 and 1.53 dB when $D = 100$ and 200 km, which are higher than about 1.45 and 1.43 dB for $D = 300$ and 400 km, respectively. The R^2 of the modeling results indicates the portion of $P(t)$ variance that can be explained by sea-ice concentration and ocean-wave activity and shows an opposite trend to RMSE across the considered ranges of D (Figure 3c, gray dashed line). The model with D of 400 km has the lowest RMSE and the highest R^2 of about 48 %, which is about 7% larger compared to that for $D = 200$ km. In the following discussion, we focus on the results with $D = 400$ km as this case best explains the microseism power.

3.2. Model Performance as a Function of Time

The results for $D = 400$ km are shown in Figure 4. In Figure 4a, the observed microseism power $P(t)$ is compared to that predicted by the model $\hat{P}(t)$ over the period 1991–2022 using the optimal $\beta_{i(i=0,1,2)}$. $\hat{P}(t)$ captures the seasonal cycle of microseism power variation relatively well, although it displays much less week-to-week variability compared to the $P(t)$. Moreover, linearly fitting $\hat{P}(t)$ over time results in a long-term trend (red line in Figure 4a) of +0.23 dB/decade (5.4%/decade since 1991). The overall increase is consistent with that of the observed $P(t)$ (gray line in Figure 4a), even though the magnitude of the increase is about a factor of 2 smaller.

To further assess how each model term contribution varies over time from 1991–2022, we evaluate ocean and sea-ice terms separately (Figures 4b and 4c). The linearly fitted long-term trend of each term shows a positive increase over time, indicating climate-induced reductions in sea-ice concentrations over the Arctic Ocean and an increase

in ocean-wave activity in this particular region. The long-term trend for the sea-ice term is 0.15 dB/decade, or about 3.5%/decade since 1991 (Figure 4b, dark blue line). This is about 2 times larger than that of the ocean term, that is 0.08 dB/decade (1.9%/decade since 1991) (Figure 4c, dark red line). This ocean energy rate of increase is of similar magnitude to large-scale ocean secular increases of several tenths of a percent per year from oceanographic (e.g., Reguero et al., 2019) and seismographic (Aster et al., 2023) estimates in recent decades. Furthermore, by calculating the range of microseism power each year and taking the average through the 32 years, we can estimate the seasonal variation of each term. In which, the sea-ice term is 3.7 dB, while the ocean term is 1.8 dB. Moreover, the variance of the sea-ice term is larger than that of the ocean term, which is about 1.1 and 0.3 respectively (Figure 3d, at $D = 400$ km). Both these long-term and seasonal variations of the two terms indicate that the contribution of the sea-ice term is about twice as large as that of the ocean term in explaining the microseism at $D = 400$ km. For smaller distance ranges ($D = 100 - 300$ km), sea-ice variation is still the dominating factor with larger variances (Figure 3d).

4. Discussion

The short-period secondary microseism is excited by ocean-wave activity which, for the Arctic Ocean, can be influenced by how sea-ice cover both impedes wind generation of waves and resists vertical movement of the ocean surface through its rigidity (Gimbert & Tsai, 2015; Montiel et al., 2022). The novel approach developed here is to parameterize the ocean-wave activity using a proxy variable $(\vec{U}_o)$ that depends on the wind-driven sea-ice drift, that is, $\mathbf{F}\vec{U}_g$ and the sea-ice motion $(\vec{U}_i)$. This proxy variable represents the ocean source of microseism energy. In practice, $|\vec{U}_o|$ has its greatest variation along the continental shelf since the ocean-wave activity is expected to have greater amplitude and complexity in shallow water areas near the coastline, as shown in previous studies (Kimura, 2004; Kimura & Wakatsuchi, 2000). This is consistent with our observation, where both the ocean-wave activity (blue line in Figure 3a) and its standard deviation (blue line in Figure S3 in Supporting Information S1) decrease with D. The standard deviation decreases most abruptly as D extends over 200 km, which marks the transition from the local continental shelf region to the deeper ocean (Figure 3e). Similarly, we find that the sensitivity of the model to the ocean-wave activity — which is quantified by the magnitude of β_1 (black line in Figure 3a) — also decreases significantly from $D = 200$ to 300 km.

Sea-ice concentration decreases with distance D except in the immediate vicinity of the coastline ($D = 100$ km) where ocean wave breaking at the shore can result in low sea-ice concentration (red line in Figure 3b). Beyond $D = 200$ km, there are relatively steep slopes in bathymetry (Figure 3e), and this can cause turbulence in the ocean, and in turn, more breaking of sea ice as we can see in both sea-ice concentration and its standard deviation (red lines in Figures 3b and Figure S3 in Supporting Information S1). The sensitivity of the microseism to sea-ice concentration, that is, β_2 (black line in Figure 3b), is also high in the distance ranges corresponding to the continental slope. These results highlight the effect of bathymetry on the ocean-wave activity, the sea-ice concentration, and the microseism.

With respect to temporal variation, the model has poorer performance when the sea-ice concentration is near 100% in wintertime (Figures 3c and 4a). This may indicate that other properties of the sea ice, such as thickness, age, snow cover, and factors that determine mechanical strength, become more important in determining the attenuation of microseism when the ocean surface is fully ice-covered. Moreover, the generation of the secondary microseism source can be dynamic on an hourly scale (Ardhuin et al., 2011). As the model input has been intentionally averaged to match the resolution of sea-ice and ocean observational data, the variation of microseism on a smaller scale is unable to be captured by the model. Since the ocean is nearly fully covered by sea ice in the winter, the microseism source in this case may have less contribution from the air-sea interaction, but more from various deep ocean wave mechanisms on a smaller scale through the generation of wave-wave interaction.

5. Conclusion

The model constructed here demonstrates that sea-ice concentration and a proxy ocean-wave activity variable, based on observed surface winds and sea-ice drift, can predict 32 years of microseism observed at a site on the coast of the Arctic Ocean with relatively high accuracy. Although this simplified linear model cannot explain the small-scale variation of microseism power, the model captures its seasonal cycle in sea-ice and ocean conditions. The model also, notably, captures the long-term secular change in microseism power due to climate change.

To the best of our knowledge, our study presents the first attempt to take into account the influence of sea-ice dynamics on sea-ice-associated microseism. Our model suggests that short-period variability of secondary microseism can be attributed to not only sea-ice concentration, as has been shown in previous studies, but also to sea-ice motion that is associated with local wind. Moreover, the modeling results depend on the spatial distribution of sea ice as well as how ocean waves are influenced by local bathymetry. A more comprehensive model and computational algorithm (e.g., Cannata et al., 2020; Minio et al., 2023; Moschella et al., 2020) should be a focus of future study, so to develop the resolution of microseism observation on the parameters that govern sea ice and ocean conditions in the Arctic. The demonstration that microseism can be used to detect and quantify sea-ice change in the Arctic Ocean presented here supports the idea that seismic observations at coastal stations can be used as a means to constrain sea-ice properties using inverse methods even in remote regions. Whether seismic observation and modeling can complement conventional sea-ice observation, such as by satellite imagery and *in-situ* monitoring, remains to be determined.

Data Availability Statement

Seismic data used in this study are available through the EarthScope Data Management Center (https://service.iris.edu) under Global Seismograph Network code II (Scripps Institution of Oceanography, 1986). Seismic data pre-processing was done using Python ObsPy Toolbox (The ObsPy Development Team, 2024). ERA5 surface wind data (Hersbach et al., 2023) are available through ECMWF data archive (https://cds.climate.copernicus.eu/datasets). Sea-ice concentration and motion data (DiGirolamo et al., 2022; Tschudi et al., 2019) are available through NASA National Snow and Ice Data Center Distributed Active Archive Center (https://nsidc.org/data/data-programs/nsidc-daac). Figures are plotted using Matlab and *M* Map Package (Pawlowicz, 2020).

Acknowledgments

Support for this research was provided by US National Science Foundation Grants (1841467 and 2336786) awarded to the University of Chicago and a student travel grant provided to JCC provided by the Bremerhaven Sea-Ice Symposium of the International Glaciological Society in 2023. Further support (especially for JCC) was provided by the Department of the Geophysical Sciences at the University of Chicago. Professor Malte Jansen is thanked for providing advice on ocean dynamics. The facilities of EarthScope Consortium were used for access to waveforms, related metadata, and/or derived products used in this study. Global Seismographic Network (GSN) is a cooperative scientific facility operated jointly by the National Science Foundation (NSF) and the United States Geological Survey (USGS). These services are funded through the Nation Science Foundation's Seismological Facility for the Advancement of Geoscience (SAGE) Award under Cooperative Agreement EAR-1724509. We thank the reviewers, Rick Aster and an anonymous referee, and the associate editor Victor Tsai for constructive criticism and suggestions which led to significant improvements in the manuscript.

References

Anthony, R. E., Aster, R. C., & McGrath, D. (2017). Links between atmosphere, ocean, and cryosphere from two decades of microseism observations on the Antarctic Peninsula. *Journal of Geophysical Research: Earth Surface*, *122*(1), 153–166. https://doi.org/10.1002/2016JF004098

Ardhuin, F., Stutzmann, E., Schimmel, M., & Mangeney, A. (2011). Ocean wave sources of seismic noise. *Journal of Geophysical Research*, *116*(C9), C09004. https://doi.org/10.1029/2011JC006952

Aster, R., McNamara, D. E., & Bromirski, P. D. (2010). Global trends in extremal microseism intensity. *Geophysical Research Letters*, *37*(14). https://doi.org/10.1029/2010GL043472

Aster, R., Ringler, A., Anthony, R., & Lee, T. A. (2023). Increasing ocean wave energy observed in Earth's seismic wavefield since the late 20th century. *Nature Communications*, *14*(6984), 6984. https://doi.org/10.1038/s41467-023-42673-w

Bromirski, P. D., & Duennebier, F. K. (2002). The near-coastal microseism spectrum: Spatial and temporal wave climate relationships. *Journal of Geophysical Research*, *107*(B8). https://doi.org/10.1029/2001JB000265

Cannata, A., Cannavò, F., Moschella, S., Di Grazia, G., Nardone, G., Orasi, A., et al. (2020). Unravelling the relationship between microseisms and spatial distribution of sea wave height by statistical and machine learning approaches. *Remote Sensing*, *12*(5), 761. https://doi.org/10.3390/rs12050761

Cannata, A., Cannavò, F., Moschella, S., Gresta, S., & Spina, L. (2019). Exploring the link between microseism and sea ice in Antarctica by using machine learning. *Scientific Reports*, *9*(1), 1–15. https://doi.org/10.1038/s41598-019-49586-z

Cathles, L. M., IV, Okal, E. A., & MacAyeal, D. R. (2009). Seismic observations of sea swell on the floating Ross Ice Shelf, Antarctica. *Journal of Geophysical Research*, *114*(F2). https://doi.org/10.1029/2007JF000934

Cessaro, R. K. (1994). Sources of primary and secondary microseisms. *Bulletin of the Seismological Society of America*, *84*(1), 142–148. https://doi.org/10.1785/BSSA0840010142

Comiso, J. C. (1986). Characteristics of Arctic winter sea ice from satellite multispectral microwave observations. *Journal of Geophysical Research*, *91*(C1), 975–994. https://doi.org/10.1029/JC091iC01p00975

Comiso, J. C., & Kwok, R. (1996). Surface and radiative characteristics of the summer Arctic sea ice cover from multisensor satellite observations. *Journal of Geophysical Research*, *101*(C12), 28397–28416. https://doi.org/10.1029/96JC02816

DiGirolamo, N., Parkinson, C. L., Cavalieri, D. J., Gloersen, P., & Zwally, H. J. (2022). Sea ice concentrations from nimbus-7 SMMR and DMSP SSM/I-ssmis passive microwave data Version 2 [Dataset]. NASA National Snow and Ice Data Center Distributed Active Archive Center. https://doi.org/10.5067/MPYG15WAA4WX

Gimbert, F., & Tsai, V. C. (2015). Predicting short-period, wind-wave-generated seismic noise in coastal regions. *Earth and Planetary Science Letters*, *426*, 280–292. https://doi.org/10.1016/j.epsl.2015.06.017

Grob, M., Maggi, A., & Stutzmann, E. (2011a). Observations of the seasonality of the Antarctic microseismic signal, and its association to sea ice variability. *Geophysical Research Letters*, *38*(11). https://doi.org/10.1029/2011GL047525

Grob, M., Maggi, A., & Stutzmann, E. (2011b). Observations of the seasonality of the Antarctic microseismic signal, and its association to sea ice variability. *Geophysical Research Letters*, *38*(11). https://doi.org/10.1029/2011GL047525

Gualtieri, L., Bachmann, E., Simons, F. J., & Tromp, J. (2020). The origin of secondary microseism Love waves. *Proceedings of the National Academy of Sciences*, *117*(47), 29504–29511. https://doi.org/10.1073/pnas.2013806117

Hasselmann, K. (1963). A statistical analysis of the generation of microseisms. *Reviews of Geophysics*, *1*(2), 177–210. https://doi.org/10.1029/RG001i002p00177

Haubrich, R. A., & McCamy, K. (1969). Microseisms: Coastal and pelagic sources. *Reviews of Geophysics*, *7*(3), 539–571. https://doi.org/10.1029/RG007i003p00539

Heorton, H. D. B. S., Tsamados, M., Cole, S. T., Ferreira, A. M. G., Berbellini, A., Fox, M., & Armitage, T. W. K. (2019). Retrieving sea ice drag coefficients and turning angles from in situ and satellite observations using an inverse modeling framework. *Journal of Geophysical Research: Oceans*, *124*(8), 6388–6413. https://doi.org/10.1029/2018JC014881

Hersbach, H., Bell, B., Berrisford, P., Biavati, G., Horányi, A., Muñoz Sabater, J., et al. (2023). ERA5 hourly data on pressure levels from 1940 to present. *Copernicus Climate Change Service (C3S) Climate Data Store (CDS)*. [Dataset]. https://doi.org/10.24381/cds.bd0915c6

Johannessen, O. M., Shalina, E. V., & Miles, M. W. (1999). Satellite evidence for an Arctic sea ice cover in transformation. *Science*, *286*(5446), 1937–1939. https://doi.org/10.1126/science.286.5446.1937

Kauker, F., Kaminski, T., Karcher, M., Giering, R., Gerdes, R., & Voßbeck, M. (2009). Adjoint analysis of the 2007 all time Arctic sea-ice minimum. *Geophysical Research Letters*, *36*(3), 3707. https://doi.org/10.1029/2008GL036323

Kimura, N. (2004). NOTES and correspondence sea ice motion in response to surface wind and ocean current in the Southern Ocean. *Journal of the Meteorological Society of Japan*, *82*(4), 1223–1231. https://doi.org/10.2151/jmsj.2004.1223

Kimura, N., & Wakatsuchi, M. (2000). Relationship between sea ice motion and geostrophic wind in the northern hemisphere. *Geophysical Research Letters*, *27*(22), 3735–3738. https://doi.org/10.1029/2000GL011495

Koch, F. W., Wiens, D. A., Euler, G. G., Aster, R. C., Nyblade, A., Anandakrishnan, S., et al. (2011). Tracking the effect of sea ice cover on microseismic noise using two seismic arrays in Antarctica. *Agu Fall Meeting Abstracts*, *2011*, S31C–S2247.

Kwok, R. (2010). Satellite remote sensing of sea-ice thickness and kinematics: A review. *Journal of Glaciology*, *56*(200), 1129–1140. https://doi.org/10.3189/002214311796406167

Lindner, F., Walter, F., Laske, G., & Gimbert, F. (2020). Glaciohydraulic seismic tremors on an Alpine glacier. *The Cryosphere*, *14*(1), 287–308. https://doi.org/10.5194/TC-14-287-2020

Longuet-Higgins, M. S., & Jeffreys, H. (1950). A theory of the origin of microseisms. *Philosophical Transactions of the Royal Society of London - Series A: Mathematical and Physical Sciences*, *243*(857), 1–35. https://doi.org/10.1098/rsta.1950.0012

Maurer, J. M., Schaefer, J. M., Russell, J. B., Rupper, S., Wangdi, N., Putnam, A. E., & Young, N. (2020). Seismic observations, numerical modeling, and geomorphic analysis of a glacier lake outburst flood in the Himalayas. *Science Advances*, *6*(38). https://doi.org/10.1126/sciadv.aba3645

Meier, W. N., Hovelsrud, G. K., van Oort, B. E., Key, J. R., Kovacs, K. M., Michel, C., et al. (2014). Arctic sea ice in transformation: A review of recent observed changes and impacts on biology and human activity. *Reviews of Geophysics*, *52*(3), 185–217. https://doi.org/10.1002/2013RG000431

Minio, V., Borzì, A. M., Saitta, S., Alparone, S., Cannata, A., Ciraolo, G., et al. (2023). Towards a monitoring system of the sea state based on microseism and machine learning. *Environmental Modelling and Software*, *167*, 105781. https://doi.org/10.1016/j.envsoft.2023.105781

Montiel, F., Kohout, A. L., & Roach, L. A. (2022). Physical drivers of ocean wave attenuation in the marginal ice zone. *Journal of Physical Oceanography*, *52*(5), 889–906. https://doi.org/10.1175/JPO-D-21-0240.1

Moschella, S., Cannata, A., Cannavò, F., Di Grazia, G., Nardone, G., Orasi, A., et al. (2020). Insights into microseism sources by array and machine learning techniques: Ionian and Tyrrhenian Sea case of study. *Frontiers in Earth Science*, *8*. https://doi.org/10.3389/feart.2020.00114

Ordoñez, A. C., Bitz, C. M., & Blanchard-Wrigglesworth, E. (2018). Processes controlling arctic and Antarctic sea ice predictability in the community earth system model. *Journal of Climate*, *31*(23), 9771–9786. https://doi.org/10.1175/JCLI-D-18-0348.1

Pawlowicz, R. (2020). M map: A mapping package for MATLAB version 1.4m [Software]. Retrieved from https://www.eoas.ubc.ca/~rich/map.html

Press, F., & Ewing, M. (1948). A theory of microseisms with geologic applications. *Eos, Transactions American Geophysical Union*, *29*(2), 163–174. https://doi.org/10.1029/TR029i002p00163

Reguero, B., Losada, I., & Méndez, F. (2019). A recent increase in global wave power as a consequence of oceanic warming. *Nature Communications*, *10*(205), 205. https://doi.org/10.1038/s41467-018-08066-0

Ricker, R., Hendricks, S., Helm, V., Skourup, H., & Davidson, M. (2014). Sensitivity of CryoSat-2 Arctic sea-ice freeboard and thickness on radar-waveform interpretation. *The Cryosphere*, *8*(4), 1607–1622. https://doi.org/10.5194/tc-8-1607-2014

Ringler, A. T., Anthony, R. E., Aster, R. C., Ammon, C. J., Arrowsmith, S., Benz, H., et al. (2022). Achievements and prospects of global broadband seismographic networks after 30 Years of continuous geophysical observations. *Reviews of Geophysics*, *60*(3), e2021RG000749. (e2021RG000749 2021RG000749. https://doi.org/10.1029/2021RG000749

Scripps Institution of Oceanography. (1986). Global Seismograph Network - iris/ida. *International Federation of Digital Seismograph Networks*. [Dataset]. https://doi.org/10.7914/SN/II

Sergeant, A., Stutzmann, E., Maggi, A., Schimmel, M., Ardhuin, F., & Obrebski, M. (2013). Frequency-dependent noise sources in the North Atlantic Ocean. *Geochemistry, Geophysics, Geosystems*, *14*(12), 5341–5353. https://doi.org/10.1002/2013GC004905

Stroeve, J., & Notz, D. (2018). Changing state of Arctic sea ice across all seasons. *Environmental Research Letters*, *13*(10), 103001. https://doi.org/10.1088/1748-9326/aade56

Stutzmann, E., Schimmel, M., Patau, G., & Maggi, A. (2009). Global climate imprint on seismic noise. *Geochemistry, Geophysics, Geosystems*, *10*(11). https://doi.org/10.1029/2009GC002619

The ObsPy Development Team. (2024). ObsPy 1.4.1 (1.4.1) [Software]. *Zenodo*. Retrieved from https://doi.org/10.5281/zenodo.11093256

Tsai, V. C., & McNamara, D. E. (2011). Quantifying the influence of sea ice on ocean microseism using observations from the Bering Sea, Alaska. *Geophysical Research Letters*, *38*(22). https://doi.org/10.1029/2011GL049791

Tschudi, M., Meier, W. N., Stewart, J. S., Fowler, C., & Maslanik, J. (2019). Polar pathfinder daily 25 km EASE-grid Sea Ice motion vectors Version 4 [Dataset]. NASA National Snow and Ice Data Center Distributed Active Archive Center. https://doi.org/10.5067/INAWUWO7QH7B

Wadhams, P., Tucker III, W. B., Krabill, W. B., Swift, R. N., Comiso, J. C., & Davis, N. R. (1992). Relationship between sea ice freeboard and draft in the Arctic Basin, and implications for ice thickness monitoring. *Journal of Geophysical Research*, *97*(C12), 20325–20334. https://doi.org/10.1029/92JC02014